Complex Fluorescence of the Cyan Fluorescent Protein: Comparisons with the H148D Variant and Consequences for Quantitative Cell Imaging[†]

Aude Villoing,[‡] Myriam Ridhoir,[‡] Bertrand Cinquin,[‡] Marie Erard,[‡] Luis Alvarez,[‡] Germain Vallverdu,[‡] Pascal Pernot,[‡] Régis Grailhe,[§] Fabienne Mérola,[‡] and Hélène Pasquier*[,‡]

Laboratoire de Chimie Physique, UMR 8000, Université Paris-Sud 11 and CNRS, Orsay 91405, France, and Institut Pasteur, 39-1 Hawolgok-dong, Seoul 136-791, Korea

Received July 25, 2008; Revised Manuscript Received October 9, 2008

ABSTRACT: We have studied the fluorescence decays of the purified enhanced cyan fluorescent protein (ECFP, with chromophore sequence Thr-Trp-Gly) and of its variant carrying the single H148D mutation characteristic of the brighter form Cerulean. Both proteins exhibit highly complex fluorescence decays showing strong temperature and pH dependences. At neutral pH, the H148D mutation leads (i) to a general increase in all fluorescence lifetimes and (ii) to the disappearance of a subpopulation, estimated to be more than 25% of the total ECFP molecules, characterized by a quenched and red-shifted fluorescence. The fluorescence lifetime distributions of ECFP and its H148D mutant remain otherwise very similar, indicating a high degree of structural and dynamic similarity of the two proteins in their major form. From thermodynamic analysis, we conclude that the multiexponential decay of ECFP cannot be simply ascribed, as is generally admitted, to the slow conformational exchange characterized by NMR and X-ray crystallographic studies [Seifert, M. H., et al. (2002) *J. Am. Chem. Soc. 124*, 7932−7942; Bae, J. H., et al. (2003) *J. Mol. Biol. 328*, 1071−1081]. Parallel measurements in living cells show that these fluorescence properties in neutral solution are very similar to those of cytosolic ECFP.

Since the discovery and cloning of the green fluorescent protein (GFP) from the jellyfish *Aequoria victoria*, fluorescent proteins (FPs)[1] have revolutionized biological imaging because of their ability to mark specified proteins and compartments in living cells (*1, 2*). Besides their widespread use as probes of protein and organelle localization, FPs have opened the way to real-time, in situ imaging of cell chemistry and biophysics, such as diffusion and transport processes, molecular interactions, local changes in pH, concentrations in metabolites, enzymatic activity, or membrane organization (*3*−*5*). A vast majority of these FP-based chemical sensing techniques make use of the FRET interaction (Förster resonance energy transfer) between two appropriate FP spectral variants (*6*). Until now, the most extensively used FRET pair has been the ECFP/EYFP couple (enhanced cyan fluorescent protein/enhanced yellow fluorescent protein), and FRET is quantified solely [in "donor only" techniques, such as fluorescence lifetime imaging microscopy (FLIM)] or partly (in ratiometric or spectral imaging techniques) from the fluorescence changes of the ECFP donor (*7, 8*).

Chemical imaging requires a truly quantitative analysis of the fluorescence signals, at accuracies which have been seldom required in conventional microscopy. A major obstacle to such quantitative imaging lies in the possible complex photophysics of the fluorescent probe, which may result in uncontrolled variations of the signal, and thus in loss of accuracy or erroneous interpretation. Unfortunately, ECFP has a relatively low brightness, shows strong environmental sensitivity, and displays the most complex fluorescence emission kinetics reported to date among common FP variants (*9, 10*). The suboptimal fluorescence properties of ECFP are major drawbacks in the current development of FP-based quantitative FRET applications. It has been reported that the single mutation H148D in ECFP leads to an increase in both brightness and average fluorescence lifetime, and to a simplification of the fluorescence decay (*11*). This has given rise to the improved Cerulean variant (carrying the additional mutations S72A and Y145A) designed for performing more quantitative FLIM-based FRET experiments (*11*−*13*).

To gain insight into the structural and dynamic determinants of their fluorescence properties, we have undertaken the detailed study of the fluorescence decays of purified ECFP and ECFP-H148D, as a function of emission wavelength, temperature, and pH. Comparison of the two proteins shows that the H148D mutation leads to a decrease in the overall efficiency of nonradiative mechanisms and to the suppression of a quenched and red-shifted substate of ECFP

[†] This work was supported by the Fondation pour la Recherche Médicale (FRM), the CNRS, the Paris-Sud 11 University, and an ACI from FNS-MENESR (DRAB).

* To whom correspondence should be addressed: Laboratoire de Chimie Physique, Bat 349, Centre Universitaire Paris-Sud, F-91405 Orsay, France. Phone: +33 1 69 15 42 04. Fax: +33 1 69 15 61 88. E-mail: pasquier@lcp.u-psud.fr.

[‡] Université Paris-Sud 11 and CNRS.

[§] Institut Pasteur.

[1] Abbreviations: ECFP, enhanced cyan fluorescent protein; ECFP-H148D, enhanced cyan fluorescent protein carrying the single H148D mutation; *Av*GFP, *Aequoria victoria* green fluorescent protein; FP, fluorescent protein; FRET, Förster resonance energy transfer; FLIM, fluorescence lifetime imaging microscopy; TCSPC, time-correlated single-photon counting; IRF, instrument response function; MCP-PMT, multichannel plate photomultiplier.

10.1021/bi801400d CCC: $40.75
Published on Web 11/01/2008

but has otherwise little structural and dynamic consequence for its major form. The emission kinetics of both proteins are in all cases very complex and sensitive to temperature and pH. Our results indicate that this complexity is not likely to arise from an excited-state relaxation or from the ground-state conformational equilibrium previously reported for ECFP (*14, 15*). It might be instead a specific property of the protein chromophore that will require new, unconventional dynamic photophysical modeling.

MATERIALS AND METHODS

Materials and Molecular Cloning. 2-(*N*-Morpholino)ethanesulfonic acid (MES; Sigma), CAPS (Sigma), and Bis-tris propane (Sigma) buffers as well as H_2SO_4 and NaOH (Aldrich) were used as received. Purified *Av*GFP was obtained from Clontech and checked for homogeneity before use by SDS−PAGE. The expression plasmid for the His-tagged ECFP (pHis-ECFP) was constructed from pECFP-N1 (Clontech) using the polymerase chain reaction (PCR). The entire ECFP sequence was amplified by PCR using the sense primer 5′-AAGGCGCCGTGAGCAAGGGCGAG-GAGCTG-3′ and the antisense primer 5′-TTAAGCTTACT-TGTACAGCTCGTCCATGCC-3′. The resulting PCR product was digested with *Ehe*I and *Hin*dIII, ligated in the pPROEX-HTa expression vector (GibcoBRL), and verified by restriction mapping and nucleotide sequencing.

Purification of ECFP and ECFP-H148D. His-tagged recombinant proteins were prepared using DH-10B cells (Invitrogen). Competent cells were transformed with the pHis-ECFP vector (*Av*GFP-F64L, -S65T, -Y66W, -N146I, -M153T, and -V163A) according to the manufacturer's protocol. The H148D mutation was introduced into ECFP using the Quickchange mutagenesis method (Stratagene). All reactions were carried out using the Pfu polymerase (Stratagene) under conditions recommended by the manufacturer. The mutation was verified by restriction endonuclease digestion and DNA sequencing. A prewarmed volume of 500 mL of Luria-Bertani (LB) broth containing 250 μg/mL ampicillin was inoculated with a 1% (v/v) starter culture that was grown overnight. Protein production was induced (OD = 0.4) using 1 mM isopropyl β-D-thiogalactopyranoside (IPTG). After being cultured for 5 h at 37 °C, cells were harvested, concentrated by centrifugation, and frozen. Later, the cells were harvested by centrifugation, resuspended in 30 mL of lysis buffer (20 mM Tris-HCl, 5 mM 2-mercaptoethanol, and 1 mM PMSF), and sonicated. The cell debris were removed by centrifugation. The supernatant was applied to a column containing 5 mL of Ni-NTA agarose (Invitrogen). The purified fusion protein His-ECFP was further concentrated, and the elution buffer was replaced with 2 mM CAPS/MES/Bis-tris propane (pH 7.4) buffer by using 10 kDa cutoff centricon columns (YM-10; Millipore). Protein concentrations were quantified using a Bio-Rad protein assay. SDS−PAGE of the purified protein shows a single band corresponding to 29 kDa, and the sample purity was assessed to be superior to 95%.

Most data reported in this work were obtained with proteins carrying the polyhistidine tag used for purification. After its removal by AcTEV-protease digestion (Invitrogen), the non-His-tagged protein displayed identical fluorescence decay curves and lifetime distributions under standard conditions.

Fluorescence Spectroscopy. All spectroscopic measurements were performed at controlled sample temperatures (±0.1 °C), using 3 mm path length quartz cuvettes with black side walls (Hellma 105-251-QS, Hellma Ltd.). Photophysical studies were conducted in an aqueous buffered solution containing 30 mM CAPS, 30 mM MES, and 30 mM Bis-tris propane, whose pH was adjusted by addition of H_2SO_4 or NaOH. The protein concentration was typically 1 μM for steady-state measurements and 10 μM for time-resolved studies. We checked that the steady-state spectra as well as the decay curves of ECFP did not depend on its concentration in the range of 1−10 μM.

For pH studies, aliquots from a concentrated protein solution were diluted into buffers previously adjusted to the appropriate pH at 20 °C (measurement accuracy, 0.1 unit). Direct addition of concentrated acid to ECFP solutions leads to irreversible aggregation of the protein and was strictly avoided. For temperature studies, the pH of the buffer was fixed to 9.0 at 20 °C. This pH undergoes a slight linear variation of <1 pH unit from 9.2 at 0 °C to 8.7 at 40 °C. Over this pH range, unlike at neutral and acidic pHs, the emission and excitation spectra of ECFP remain unchanged, and the lifetime distributions exhibit only little perturbation (see Results). Therefore, modifications in the fluorescence decay kinetics observed over this temperature range can be considered to result only from the temperature dependence of the ECFP fluorescence.

(i) Steady-State Fluorescence. UV−visible spectra were recorded on a Perkin-Elmer Lambda 900 spectrophotometer. The steady-state emission and excitation spectra were recorded on a Spex Fluorolog 1681 spectrofluorimeter. Band widths of 0.9 nm for excitation and emission were used. Spectra were collected with integration set to 1 s and an increment of 1 nm. In all experiments, a signal from pure buffer was subtracted as a background. The maximal average power at the sample was 18 ± 2 μW, with a beam section of ∼0.15 cm^2.

(ii) Time-Resolved Fluorescence. The fluorescence decay curves were recorded using the time-correlated single-photon counting technique (TCSPC) (*16*) with, as an excitation source, a mode-locked tuneable Ti:sappphire laser (MIRA 900, Coherent) pumped by a solid-state diode laser (10 W Verdi, Coherent). The laser repetition rate of 76 MHz was reduced to 3.8 MHz using a pulse picker (SiO_2 crystal, APE). The excitation wavelength was 420 nm obtained by frequency doubling the 840 nm laser radiation after the pulse picker using an angle-tuned LBO crystal. After the frequency doubler, the laser excitation light was directed unfocused on the sample placed in a temperature-controlled multiposition sample holder. The average laser power at the sample was typically 1−3.5 μW (beam waist of ∼1−2 mm). The fluorescence decay curves were collected using a fast MCP-PMT (Hamamatsu) and standard high-grade TCSPC electronics (Ortec, Phillips & Tennelec). The instrumental response function (IRF) obtained by measuring the light scattered from a LUDOX solution (Dupont) was typically 60−70 ps full width at half-maximum, as accumulated during a complete experiment. The excitation was vertically polarized, and the sample fluorescence was passed through a

polarizer oriented at the magic angle (54.7°) prior to the emission monochromator. The monochromator band path was 6 nm for most experiments, except for pH and temperature studies on ECFP-H148D, where it was 24 nm. The fluorescence from the sample and the IRF are collected alternately over several tens of cycles to average out small fluctuations and to reach sufficient statistics: typically 15−25 $\times$ 10^6 total counts were collected in each decay curve, at rates of $\sim 10^4$ counts/s.

(iii) Photobleaching. ECFP has been reported to undergo both reversible and irreversible slow photobleaching reactions, particularly at acidic pHs (*17*). Therefore, photoreactions were carefully controlled in all steady-state and time-resolved fluorescence experiments. The excitation densities used were in all cases maintained below 10^{-3} W/cm^2, while the collection of fluorescence decays was combined with real-time monitoring of the average decay time position and intensity of the fluorescence during data acquisition. Some signal drifts were observed at pH 5.5, and thus, any experiment showing more than 10% intensity loss or 50 ps time drift over the complete data acquisition was discarded. We have checked that such limited drifts resulted in undetectable modifications of the measured average fluorescence lifetime. In the case of ECFP-H148D, acidic pH values of <6 were associated in addition with some protein aggregation, as detected by increases in light scattering.

(iv) Fluorescence Lifetime Microspectroscopy. The high-resolution fluorescence decays of ECFP expressed in HEK293 cells were measured at room temperature (21−24 °C) using the TCSPC technique under two-photon excitation, as described in ref *18*. The statistic of the collected decays was $\sim 2 \times 10^6$ total counts. The IRF was obtained by detecting second harmonic generation from a BBO crystal placed at the sample stage. Data analysis was then performed in the same way as for solution studies (see below). The intracellular temperature and pH changes of ECFP fluorescence lifetimes were studied in living CHO and PLB985 cells, respectively, using the confocal FLIM system LIMO (Nikon) as described in ref *18*.

Data Analysis. Each experimental fluorescence decay curve [$F(t)$] was analyzed individually together with its IRF using the maximum entropy method as described in ref *19*. This analysis assumes that the experimental decay $F(t)$ is the convolution product:

$$F(t) = (g * \mathrm{Im})(t) \tag{1}$$

where g is the measured IRF and Im is the pure fluorescence decay law for instant excitation. The analysis assumes that the fluorescence decay law is the sum of a large number of exponential terms. The total decay is then given by

$$\mathrm{Im}(t) = I_0 \int_0^\infty a(\tau) \mathrm{e}^{-t/\tau}\, \mathrm{d}\tau \tag{2}$$

where $a(\tau)$ is the distribution of normalized pre-exponential amplitudes [i.e., $\int a(\tau)\, \mathrm{d}\tau = 1$] and I_0 is an arbitrary factor incorporating the instrumental conditions of the measurement. A time shift between the fluorescence decay and its corresponding IRF was optimized for each experiment, to take into account small variations in optical delays. The goodness of fit was judged by the value of the reduced χ^2 which was comprised between 0.97 and 1.05, as well as by visual inspection of both the normalized residuals and the autocorrelation function, which were in all cases randomly distributed around zero (see ref *20* for details). The fluorescence decay curves could be satisfactorily fit in all cases starting from approximately half of the rising edge of the decay.

From the fluorescence lifetime distribution $a(\tau)$ recovered by this method, a small number of individual components (τ_i) and their corresponding pre-exponential amplitudes (c_i) can be obtained by partial integration over each separate peak that can be observed in the distribution, as described in ref *19*. The distribution $a(\tau)$ also allows the computation of the average fluorescence lifetime ($\langle\tau_\mathrm{f}\rangle$), defined as the amplitude-averaged decay time (*21*):

$$\langle\tau_\mathrm{f}\rangle = \sum_i c_i\tau_i = \int_{\tau=0}^{\tau=\infty} a(\tau)\tau\, \mathrm{d}\tau \tag{3}$$

This average lifetime is proportional to the steady-state fluorescence intensity that would be measured under the same experimental conditions, which can be obtained by integration over time of the fluorescence decay:

$$\int_{t=0}^{t=\infty} \mathrm{Im}(t)\, \mathrm{d}t = I_0 \int_{t=0}^{t=\infty} \int_{\tau=0}^{\tau=\infty} a(\tau) \exp^{-t/\tau}\, \mathrm{d}\tau\, \mathrm{d}t = I_0 \int_{\tau=0}^{\tau=\infty} a(\tau)\tau\, \mathrm{d}\tau \tag{4}$$

$\langle\tau_\mathrm{f}\rangle$ defined in this way is thus the most relevant quantity for lifetime-based FRET quantifications. The experimental errors on c_i, τ_i, and $\langle\tau_\mathrm{f}\rangle$ are standard deviations over repeated identical experiments.

RESULTS

Complex Fluorescence of Purified ECFP. We have performed time-resolved fluorescence spectroscopy at high statistics and time resolution of purified ECFP at pH 7.4 and 20 °C (Figure 1). Using the maximum entropy method of data analysis, a broad distribution of fluorescence lifetimes is necessary to achieve a good fit of the fluorescence decays (Figure 2a). This distribution is dominated by a well-defined long component, peaking at 3.86 $\pm$ 0.10 ns, having a barycenter located at 3.63 $\pm$ 0.12 ns, which is associated with the largest amplitude (52 $\pm$ 7% for a detection at 474 nm). This long component is flanked by a contiguous series of shorter components which span the whole range of experimentally accessible lifetimes down to a few tens of picoseconds. The values and relative amplitudes of these short components are less accurate but remain quite reproducible for fixed conditions of detection wavelength, pH, and temperature (Table 1 and Figure 2a).

The fluorescence emission kinetics of ECFP, as described by an unconstrained series of exponential terms, appears thus very complex. On the other hand, by using alternative methods of data reduction and modeling, we found that indeed, other nonexponential functions can fit our data at least equally well (unpublished results). Therefore, the fluorescence lifetime distributions reported here should be taken as a phenomenological, ad hoc description of the data, belonging to a much larger "feasible set" of solutions which remains to be explored (*19, 22*). Nevertheless, the good residuals and χ^2 obtained warrant that these multiexponential models, independent of their physical basis, are an accurate

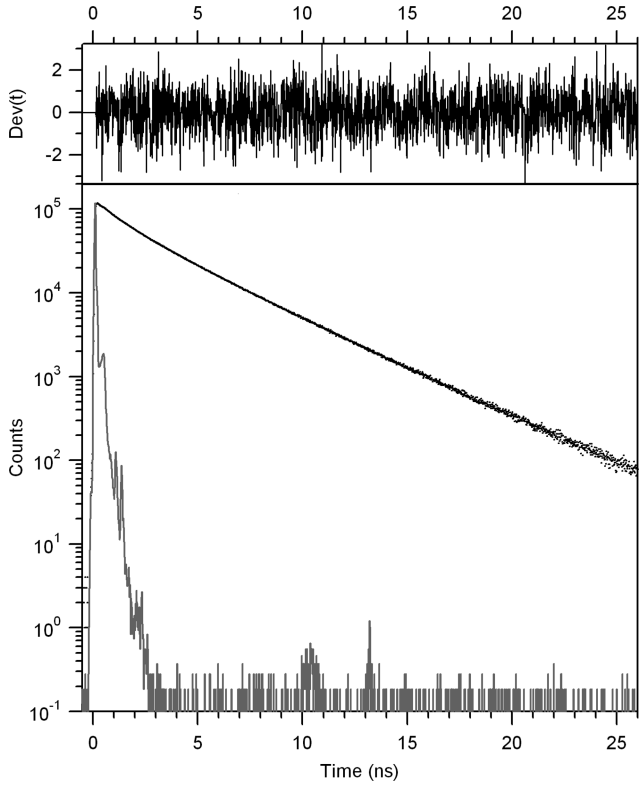

FIGURE 1: Fluorescence decay of ECFP at 20 °C and pH 7.4 (•) with corresponding instrumental function (gray line) and residuals of the fit (black line).

representation of the experimental decay profiles (Figure 1). In particular, the average fluorescence lifetime $\langle\tau_f\rangle$ defined by eq 3 (Materials and Methods), which corresponds to the time-integrated area of the decays, should be a quantity independent of the model used.

This average fluorescence lifetime is 2.52 ± 0.04 ns when the ECFP emission is detected at its maximum at 474 nm. However, this value is significantly dependent on the detection wavelength and decreases to 2.34 ns at 500 nm and 2.24 ns at 530 nm. This decrease in the average fluorescence lifetime when going from the short to the long emission wavelengths (Figure 3a) was previously unnoticed by other authors (*10*). At all emission wavelengths, the distributions of ECFP fluorescence lifetimes display, within errors bars, the same subcomponents (see the Supporting Information).

The average fluorescence lifetime of purified ECFP at neutral pH is in good agreement with those reported for free cytosolic ECFP expressed in living cells (*9, 13, 18, 23, 24*). Moreover, we have determined the fluorescence lifetime distribution of cytosolic ECFP expressed in living HEK293 cells (Figure 2b) using two-photon microscopy combined with TCSPC detection. Although in this case the statistics of the data that could be collected were significantly reduced (see Materials and Methods), the recovered distribution of fluorescence lifetimes is very similar to that observed for the isolated purified protein. The reduced value of all components and of the average lifetime (2.33 ns) might be due to a slightly higher refractive index in the cytosol (*25*) and/or to a slightly higher sample temperature in this experiment (see below).

Fluorescence Decays of Purified ECFP-H148D. The fluorescence decays of purified ECFP-H148D were measured and analyzed in the same way as for ECFP. The major features of the fluorescence lifetime distribution are quite similar to those of ECFP (Figure 2c). The distribution is again dominated by a long, well-defined component, which is now peaking at 4.14 ± 0.10 ns (barycenter at 4.00 ± 0.10 ns), is associated with the largest amplitude (69 ± 5%), and is followed by several shorter components. The balance is now more in favor of this long component, with all short lifetimes having reduced relative amplitudes (Figure 2c). In addition, all lifetime components appear to be shifted to higher values as compared to their possible equivalent in ECFP (Table 1 and Figure 2c). Because of its very small contribution, the shortest component is very inaccurate, and sometimes absent from the distribution. Therefore, a similar complex pattern of fluorescence lifetimes is observed for ECFP-H148D as compared to ECFP, with a persistent series of short components. This result is in no way a consequence of instrumental or methodologic biases, since, for example, the fluorescence emission kinetics of *Av*GFP measured and analyzed by the same methods appears as a nearly pure single exponential (Figure 2d), with a decay time of 3.25 ± 0.05 ns at 20 °C and pH 8.

The average fluorescence lifetime of ECFP-H148D computed at pH 7.5 ± 0.5 and 20 °C is 3.32 ± 0.04 ns, which is consistent with the increased quantum yield of this variant as compared to that of ECFP (*11*). However, by contrast to that of ECFP, we found that the average fluorescence lifetime of ECFP-H148D is nearly invariant with the detection wavelengh in the range of 460−560 nm (Figure 3b).

Fluorescence Decays of ECFP and ECFP-H148D versus Temperature. As a general rule, the fluorescence intensity and lifetime of most chromophores are expected to decrease when the temperature is increased, because the nonradiative deexcitation paths (which compete with the radiative process) are usually controlled by activation barriers. We have studied the temperature dependence of the fluorescence decays of purified ECFP between 0 and 40 °C in a buffer adjusted to pH 9.0 at 20 °C (see Materials and Methods). We found that the average fluorescence lifetime displays an unusual strong temperature dependence, with a roughly linear decrease of ~0.048 ns/°C (Figure 4). Similarly, the fluorescence lifetime of cytosolic ECFP in living cells decreases by ~0.043 ns/°C (data not shown).

In the case of purified ECFP, this effect arises first from the expected temperature-induced decrease of all ECFP lifetime components but also, and more importantly, from a strong decrease in the relative amplitude of the long component, which typically decreases from 72% at 0 °C to 30% at 40 °C, while the amplitudes of all short lifetimes increase concomitantly. These strong perturbations of the fluorescence decays are accompanied by only small changes in the shape of the emission spectrum (data not shown), while the steady-state fluorescence intensity closely parallels the changes in fluorescence lifetime (Figure 4). All temperature-induced changes are fully reversible over the temperature range explored. In the case of purified ECFP-H148D, the average fluorescence lifetime decreases also rapidly and reversibly with an increase in temperature, by ~0.044 ns/°C (Figure 4). This decrease arises again in large part from a decrease in the relative amplitude of the long fluorescence lifetime (from 85% at 0 °C to 47% at 40 °C). Again, the fluorescence emission spectrum of ECFP-H148D displays

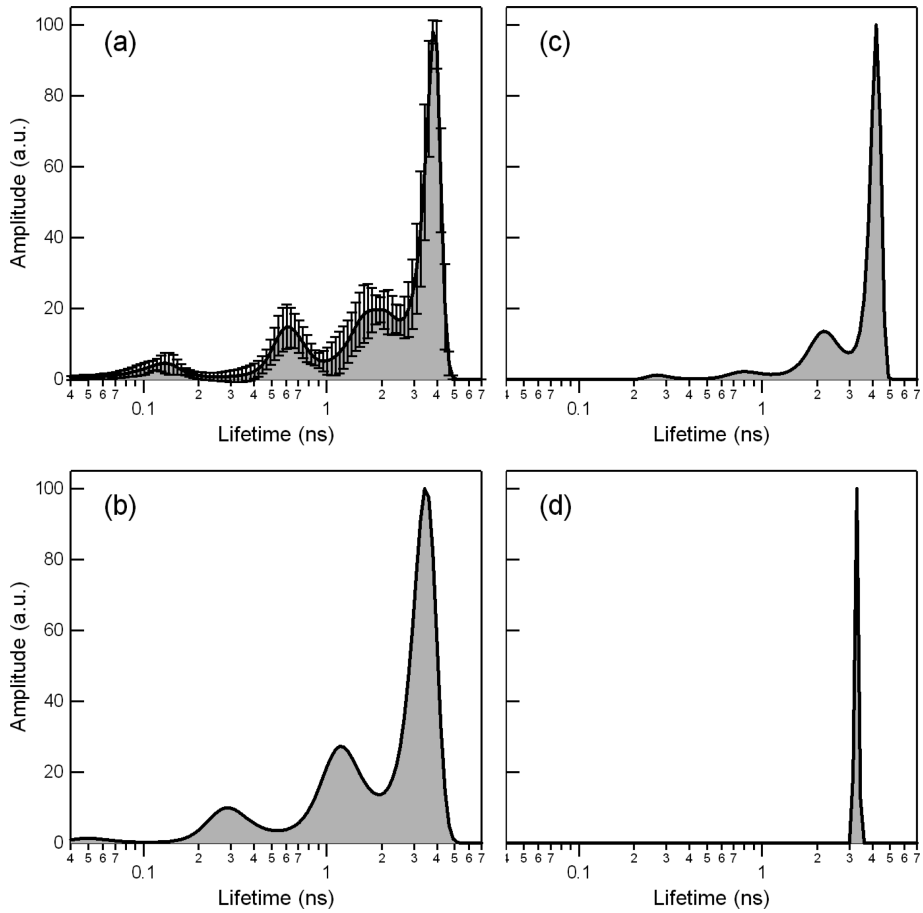

FIGURE 2: Distribution of fluorescence lifetimes obtained from fluorescence decay analysis of (a) purified ECFP, (b) cytosolic ECFP in HEK23 cells, (c) purified ECFP-H148D, and (d) *Av*GFP. The distribution shown for purified ECFP is an average of six independent experiments, and error bars represent the standard deviation between these distributions.

Table 1: Fluorescence Lifetime Components of ECFP and ECFP-H148D at 20 °C

	ECFP[a]		ECFP-H148D[b]	
	τ_i (ns)	σ_i (ns)	τ_i (ns)	σ_i (ns)
τ_1	0.12	0.04	<0.5	na
τ_2	0.61	0.1	0.78	0.2
τ_3	1.75	0.3	2.02	0.2
τ_L	3.63	0.1	4.00	0.1

[a] At pH 7.4 and 20 °C with $\lambda_{exc} = 420$ nm and $\lambda_{em} = 474$ nm ($\Delta\lambda_{em} = 6$ nm). [b] At pH 7.5 ± 0.5 and 20 °C with $\lambda_{exc} = 420$ nm and $\lambda_{em} = 474$ nm ($\Delta\lambda_{em} = 24$ nm).

only weak perturbations over this temperature range (data not shown), while the steady-state intensity decreases with temperature in proportion to the average lifetime (Figure 4).

Deviations from strict proportionality between the average fluorescence lifetime and the steady-state intensity and fluorescence quantum yield either would indicate the existence of a variable proportion of nonfluorescent molecules, undergoing static or highly efficient dynamic quenching, or might manifest some changes in the radiative rate of the chromophore (*19, 21, 26*). Indeed, the fact that this proportionality is verified for ECFP as well as for ECFP-H148D, in the presence of large amounts of short lifetimes under certain temperature conditions, demonstrates the absence of significant exchange with nonfluorescent populations in both proteins.

pH Dependence of the Fluorescence Decays of ECFP and ECFP-H148D. It was shown earlier that an acidification of the medium leads to a strong decrease in the fluorescence intensity of ECFP (*27*). The transition point for this intensity change is around pH 5 (*28*). This decrease is accompanied by profound changes in the shape of the ECFP emission spectrum, with a loss of its charateristic double-hump structure and a red shift of 6 nm of the emission maximum, while the absorption spectrum shows only limited perturbations (*17*). We measured the fluorescence decays of ECFP at high statistics from pH 11 to 5.5. The photosensitivity of ECFP at acidic pH values precluded accurate measurements at lower pH values (see Materials and Methods). We find that a decrease in pH below neutral leads to a rapid decrease in the ECFP average fluorescence lifetime, of ~10% at pH 6.5 and ~40% at pH 5.5 (Figure 5). Along this transition, the fluorescence emission kinetics can be described by varying weights of similar lifetime components (see the Supporting Information). The decrease in average lifetime is mostly due to a dramatic reduction in the relative amplitude of the long component, which goes from 57% at pH 11 to 14% at pH 5.5. Provided that any significant ECFP photoreaction is carefully avoided, these acid-induced changes are fully reversible after the sample returns to neutral pH. In the high-pH range, after a short plateau in the neutral region, a smooth increase in average fluorescence lifetime is observed up to pH 11 (Figure 5), a change that is also reversed by returning to neutral conditions. In living cells, we observed that the intracellular fluores-

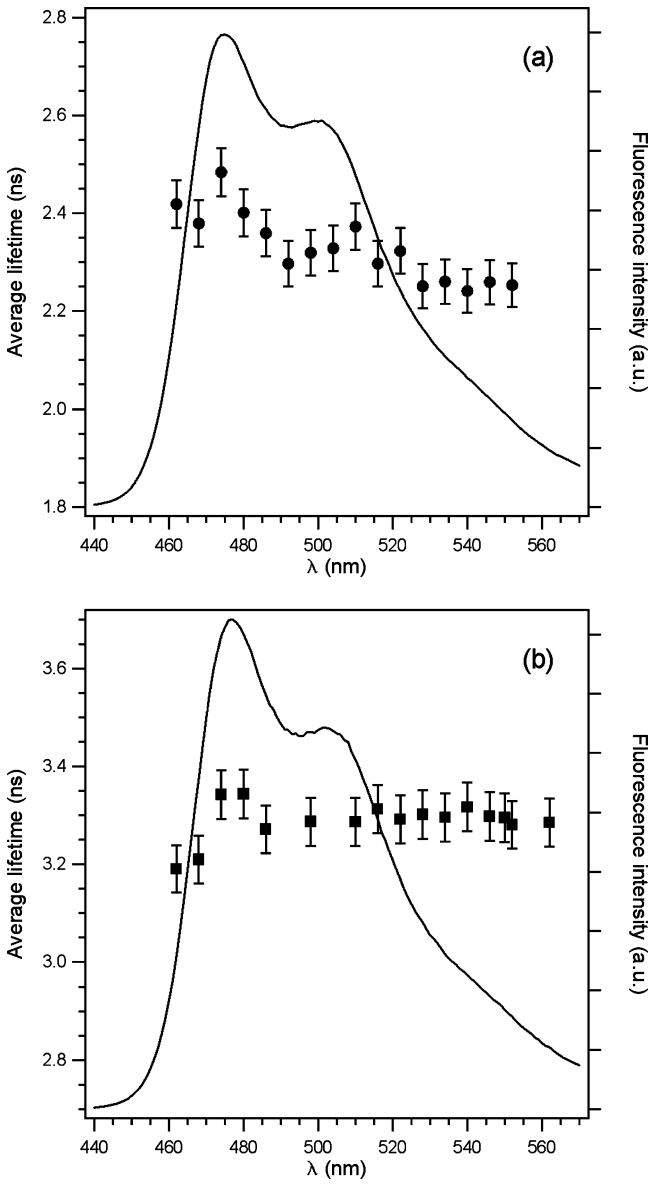

FIGURE 3: Variations of the average fluorescence lifetime with the emisson wavelength, and fluorescence emission spectrum of (a) purified ECFP and (b) purified ECFP-H148D at pH 7.4 and 20 °C. Errors bars correspond to the 1.5% standard deviation on average lifetimes established from repeated experiments.

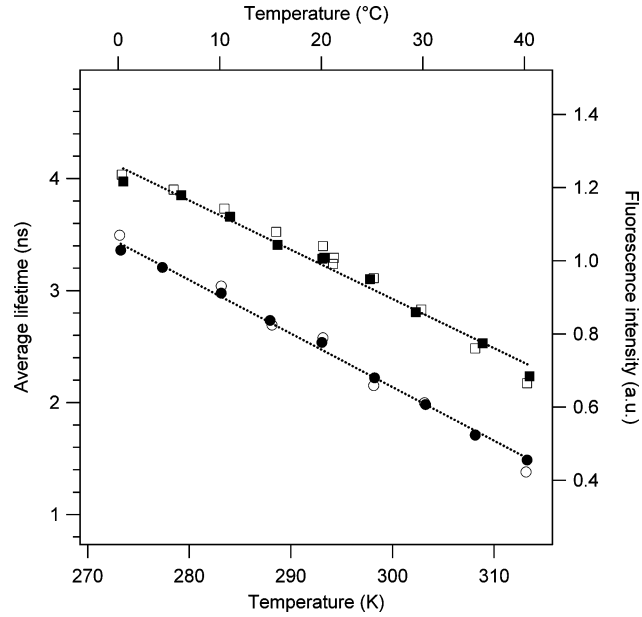

FIGURE 4: Temperature dependence of the average fluorescence lifetimes (left axis, filled symbols) and fluorescence emision intensities (right axis, empty symbols) of ECFP (circles) and ECFP-H148D (squares) at pH 9. Intensities were integrated over the whole emission spectra and scaled to the respective values of the fluorescence lifetimes at 20 °C.

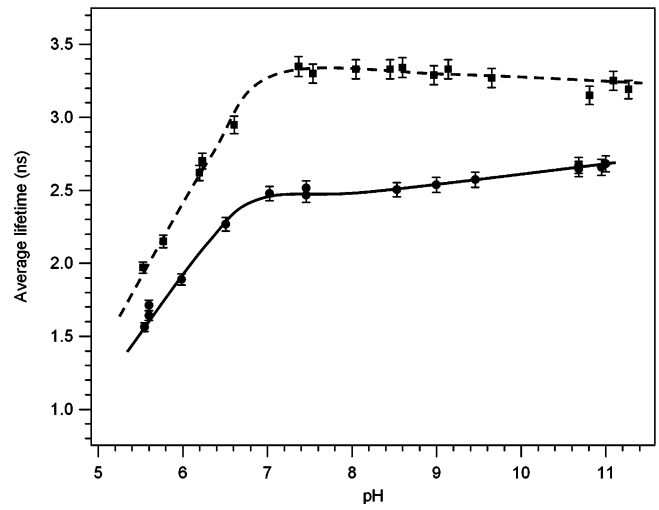

FIGURE 5: pH dependence of the average fluorescence lifetime of ECFP (●) and ECFP-H148D (■) at 20 °C. Solid and dashed lines for eye guidance only.

cence lifetime of ECFP drops by approximately 25% when the intracellular pH is decreased by cell incubation in a MES buffer at pH 5.8, in the presence of 10 μM nigericine (data not shown). This lifetime decrease is fully reversed when the acidic incubation buffer is replaced with a neutral one, provided that sample illumination is carefully avoided.

Prominent fluorescence perturbations at acidic pHs have also been reported in the case of purified Cerulean: strong and reversible shifts in both absorbance and fluorescence excitation spectra, associated with a 4-fold decrease in fluorescence intensity, take place when the pH is decreased from 8 to 5 (*29*). The pH-induced transition of Cerulean absorption and fluorescence is very slow, with a time constant on the order of 1 h, and was ascribed to a major conformational change (*29*). We studied the pH dependence of ECFP-H148D fluorescence fully equilibrated (24 h) in buffers prepared at different pHs between 5.5 and 11. A strong decrease of the average fluorescence lifetime of ECFP-H148D is observed when the pH is changed from neutral to acidic (Figure 5). In the high-pH range, with a behavior opposite with respect to that of ECFP, the average lifetime of ECFP-H148D shows a continuous decrease when the pH becomes more basic (Figure 5). As for ECFP, the fluorescence decays of ECFP-H148D measured at all pHs are described well by varying amplitudes of similar lifetime components (see the Supporting Information). More precisely, the decrease observed in the average fluorescence lifetime can be mostly associated with a decrease in the relative amplitude of the long 4 ns component, going from ~70% at neutral pHs to only 30% at pH 5.5 and 60% at pH 11.

DISCUSSION

Heterogeneous Fluorescence of ECFP. It is now fully acknowledged that ECFP has a complex, heterogeneous fluorescence: while its fluorescence decays recorded in living cells are often fit by a biexponential law (*9, 13, 18, 23, 24*), this decay was reported by Habuchi and colleagues (*10*) to be composed of at least three exponentials for the isolated protein in vitro. We report here on two different manifestations of the complex nature of this fluorescence at neutral pH: (i) the nonexponential (or highly multiexponential) emission kinetics of purified ECFP and (ii) the spectral dependence of this emission kinetics, with an acceleration of the fluorescence decay when going to the red edge of the emission spectrum.

Complex fluorescence of chromophores is usually a consequence of the multiplicity of emissive excited states, which may arise either from chemical and physical equilibria preexisting in the ground state (such as conformations or protonation states) or from reactions specifically triggered in the excited state (such as solvent dielectric relaxation or excited-state chromophore tautomerization, twisting, charge transfer, etc.), if the latter take place significantly on the nanosecond time scale. In turn, heterogeneous fluorescence emission usually implies a strong and complex environmental sensitivity of the probe, since any equilibrium shift or change in the relative detection of the different emissive forms will result in changes in the observed average signal. Therefore, understanding the origin of the fluorescence heterogeneity in ECFP can be critical in the rational design of better fluorescent proteins for quantitative imaging. First, because of the low protein concentrations and excitation power used in this study, trivial causes of fluorescence heterogeneity, such as protein dimerization (*30*) and light-induced photoconversion (*17*), can be clearly ruled out in this case.

In excited-state reactions, the excited system relaxes from the higher-energy to the lower-energy emissive states. As a result, faster fluorescence decays (shorter fluorescence lifetimes) are usually associated with blue emission, while detection on the red edge of the spectrum normally results in a slower decay (longer fluorescence lifetimes), associated with a rising exponential term reflecting the transient buildup of the new relaxed emissive form. This is verified, for example, in the case of time-dependent excited-state solvation in a viscous matrix (*31*), as well as for intra- or intermolecular excited-state proton transfer (*32*) or for many excited-state twisting processes (*33*). The characteristics of the ECFP fluorescence decays clearly do not correspond to this picture, with short lifetimes, but no detectable rising component, associated on the contrary with the low-energy side of the emission spectrum. This rules out an important contribution of excited-state relaxations in the nanosecond photophysics of ECFP.

Simpler yet Complex Fluorescence of ECFP-H148D. On the other hand, it is commonly assumed that the coexistence of two ECFP conformations found in ^{19}F NMR (*15*) and X-ray crystallographic studies (*14*) is the primary cause of the complex fluorescence emission kinetics of this protein (*13, 25, 34, 35*). The main structural change between the two conformations is an alternate displacement of the His148 and Tyr145 side chains (Figure 6). In the major ECFP conformation, His148 is located away from the chromophore

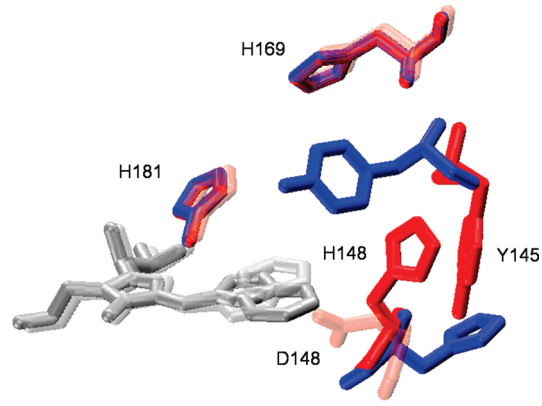

FIGURE 6: Relative positions of nearby titratable side chains in the chromophore region of the two conformations of ECFP (blue, major conformation A′; red, minor conformation B′) and in Cerulean (transparent orange), according to X-ray crystallographic structures (*14, 29*). Alignement of the three structures was achieved along the peptide backbone.

on the exterior of the protein, while in the minor conformation, it stays at the entrance of the chromophore pocket, on the protein surface. The H148D mutation was aimed at suppressing this conformational equilibrium, and actually this variant, like Cerulean, indeed has a more homogeneous and more intense fluorescence than ECFP (*11*−*13*).

Our high-resolution data provide more insights into the improved fluorescence properties of ECFP-H148D. The increase in all fluorescence lifetimes shows that the mutation has first removed a general dynamic quenching of the ECFP chromophore. This general increase leads to a first 17% increase in the average fluorescence lifetime. On the other hand, the improved fluorescence homogeneity of ECFP-H148D is characterized by a decrease in the relative weight of the short fluorescent lifetimes present in ECFP, accompanied by apparently more similar emission spectra of the remaining species. Taken together, this indicates that one or more species associated with a fast emission kinetics and a red-shifted emission spectrum have disappeared after the H148D mutation. Assuming that this red-shifted species has no contribution to the longest fluorescence lifetime of ECFP sets a minimum of ∼25% to its molar fraction (see below). This value is quite significant and might well correspond to one of the conformations identified from X-ray and NMR data (*14, 15*). The suppression of this quenched population leads to a further 16% increase in average fluorescence lifetime. Therefore, the two mechanisms contribute nearly equally to the overall increase in fluorescence associated with the H148D mutation.

Nevertheless, the emission kinetics of ECFP-H148D remains very complex and actually quite similar to that of ECFP. Whatever the underlying photophysics, the fluorescence lifetime distribution of a protein fluorophore is a highly specific and sensitive signature of local folding and physicochemical status (*26, 36, 37*). The high degree of similarity of the complex fluorescence lifetime distributions of ECFP and ECFP-H148D must reflect the high degree of structural and dynamic similarity of the two proteins in the vicinity of their chromophore. Recently, an X-ray crystallographic structure of Cerulean was obtained at acidic pHs, showing an unusual cis-coplanar conformation of the chromophore, and a buried configuration of the Asp148 side chain, interacting directly with the indole moiety of the chro-

mophore (*29*). From the fluorescence lifetime distributions of ECFP-H148D, it seems unlikely that such a peculiar configuration takes place in this variant over the neutral to basic pH range.

Thermodynamic Analyses of ECFP and ECFP-H148D Fluorescence. The complex fluorescent decays of ECFP and ECFP-H148D both comprise two major kinetic groups: a long well-defined fluorescence lifetime on one hand and a broad distribution of faster components on the other. At 20 °C and at neutral pH in ECFP, their respective average lifetimes of 3.6 and 1.3 ns correspond well to the two exponentials usually reported in the litterature for this protein. In temperature studies, strong exchanges take place in their relative amplitudes. If, as is usually assumed, these two major fluorescence decay components do arise from the slow (millisecond) conformational equilibrium of ECFP reported from NMR and X-ray crystallography (*14, 15*), their thermodynamic analysis should provide parameters consistent with those obtained from NMR data (*20*). In a situation of slow exchange, the pre-exponential amplitudes (c_i) of the different lifetime components are related to the molar fractions (x_i) of each corresponding species as follows (*38*):

$$c_i = \frac{x_i \varepsilon_i f_i k_{ri}}{\sum_i x_i \varepsilon_i f_i k_{ri}} \quad (5)$$

where ε_i is the molar absorption coefficient, f_i the detected fraction of the emission spectrum (i.e., the probability of photon emission within the detected wavelength range), and k_{ri} the radiative rate of species *i*. Since the excitation and emission spectra show only limited modifications with temperature, while the apparent radiative rates of both ECFP and ECFP-H148D do not change significantly, the pre-exponential amplitude (c_L) of the long fluorescence lifetime provides a direct estimate of the relative molar fraction (x_L) of the possible corresponding species. The variation of x_L with temperature can then be used to evaluate the thermodynamics of the equilibrium involved, according to

$$K_{eq} = \frac{1 - x_L}{x_L} = \exp^{-\Delta G_0 / RT} \quad \ln(K_{eq}) = -\frac{\Delta H_0}{R}\left(\frac{1}{T}\right) + \frac{\Delta S_0}{R} \quad (6)$$

A linear fit of $\ln(K_{eq})$ versus $1/T$ (Figure 7) yields the following values for the molar enthalpy and entropy differences of the equilibria: for ECFP, $\Delta H_0 = 33 \pm 3$ kJ/mol and $\Delta S_0 = 112 \pm 10$ J K^{-1} mol^{-1}; for ECFP-H148D, $\Delta H_0 = 38 \pm 6$ kJ/mol and $\Delta S_0 = 123 \pm 10$ J K^{-1} mol^{-1}. These thermodynamic parameters are approximately 2 times higher than those obtained from the ECFP tryptophan resonances in ^{19}F NMR spectra (*15*). Actually, the strong temperature dependence of the fluorescence decays leads to a complete inversion between the major and minor lifetime components between 0 and 40 °C, while NMR and crystallographic studies assume the same major conformation of ECFP from cryogenic temperatures to 40 °C. This shows that, contrary to what is commonly accepted, the two major kinetic groups in ECFP fluorescence decays cannot be ascribed to its two conformers reported from NMR and X-ray crystallography.

Interestingly, these two kinetic groups appear also largely disconnected from the peculiar double-hump shape of the ECFP spectra, which has been sometimes taken as a mark

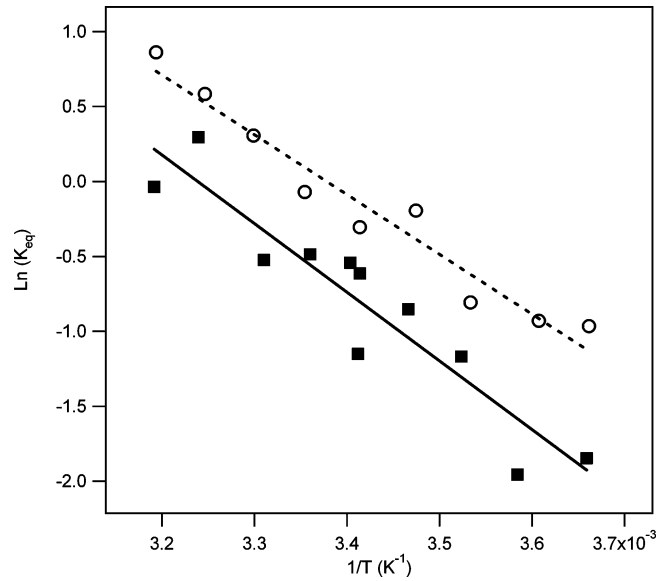

FIGURE 7: Linear fits of $\ln(K_{eq})$ vs $(1/T)$ as obtained from the pre-exponential amplitude (c_L) of the long fluorescence lifetime of ECFP (○) and ECFP-H148D (■) at pH 9.

of ground-state heterogeneity. In line with the conclusions reached about its absorption spectrum (*39, 40*), it is more likely that the two bands in the ECFP emission spectra arise from the vibrational features of a single electronic transition. Recently, it was found that this double-hump shape can be confered to the electronic spectra of a distant FP coral variant by the mere reintroduction of the Y67W mutation (*41*).

pH-Induced Changes in the Fluorescence of ECFP and ECFP-H148D. It is known that, when the pH is changed from neutral to acidic, a strong quenching and major spectral shifts of the ECFP fluorescence occur. One could speculate that the protonation state of His148, which, in both crystallographic conformers of ECFP, is one of the closest titratable residue in the vicinity of the chromophore (Figure 6), is a major determinant of these perturbations. Indeed, we find that the H148D mutation changes markedly the pH responses of the fluorescence signals. However, we observe an equivalent decrease in the fluorescence lifetime of ECFP-H148D in a similar pH range.

Protonated histidine was shown to be the second most efficient amino acid side chain (after cysteine bridges) in the quenching of tryptophan fluorescence, by a mechanism that involves mostly excited-state electron transfer, while the neutral imidazole ranges on the contrary among the weaker quenchers, showing a 65-fold lower quenching rate constant (*42*). Assuming similar nonradiative mechanisms for the ECFP chromophore implies that any change in the protonation state of a nearby histidine residue should lead to marked variations in its fluorescence intensity. The similar pH response observed after the mutation of His148 suggests that either this residue does not change its protonation state in the acid to neutral pH range or some other residues relay the quenching by His148 after its mutation. Aside from His148, His181, within ~7.5 Å of the chromophore, and His169, within >9 Å, are the next two histidines present in the chromophore's surroundings. These two residues have nearly identical positions and hydrogen bonding status in both ECFP conformations, as well as in the acid structure of Cerulean (Figure 6), which implies that their protonation

properties should not be substantially modified also in ECFP-H148D. Protonation of the nearby Tyr145 might be another cause of pH-dependent quenching, particularly in the major ECFP conformation where the residue is more buried and could display a pK_a shifted to lower values. However, the acid pH behavior of Cerulean, where this residue is mutated to an alanine, is very similar to that of ECFP-H148D (*28*), which seems to rule out a significant role for this residue in the observed pH dependence. Finally, the protonation of carboxylic acids is also expected to lead to pH-dependent quenching. In the acid structure of Cerulean, Asp148 is protonated and interacts directly with the chromophore, which makes it a possible candidate for the strong acid-induced quenching of ECFP-H148D.

Actually, it appears to be quite difficult to rationalize the complex pH responses of both ECFP and ECFP-H148D fluorescence on the basis of the titration of a few well-identified residues. Multiple transitions that extend over broad pH domains are observed, which may be the mark of possible strong correlations between titratable side chains (*43*). In addition, it has been reported that, in several GFP-derived fluorescent proteins, including ECFP, acid pHs are coupled to major conformational changes, in some cases involving cis−trans isomerization or nonplanar configurations of the chromophore itself (*17, 29, 44*). These major structural events could well be the cause of the general quenching of FPs at acidic pHs. A study of the pH behavior of non-titratable mutants of His148 in ECFP would help in deciphering the complex interplay between direct electrostatic effects and conformational changes in this protein.

Photophysics and Kinetic Modeling of ECFP Fluorescence. From all the considerations mentioned above, we must conclude that the kinetic complexity of the ECFP fluorescence decays cannot be reconciled with any of the slow physical or chemical equilibria currently described for this protein (*14, 15, 17, 27, 29*). In the mutant ECFP-H148D, after the disappearance of a red-shifted and quenched component possibly related to one conformer of ECFP, the fluorescence emission remains characterized by the same nonexponential fluorescence decay, associated with a characteristic double-hump emission spectrum, and this is true even under conditions which should strongly favor a single protein substate, i.e., when low temperature and high pH are combined.

We know that this complex kinetics is strongly sensitive to temperature and (in the neutral to basic pH range) moderately sensitive to pH, which shows that the multiple configurations that underlie this complexity must be under dynamic exchange. It is possible that these configurations arise from some other, yet unidentified, slow conformational substates of the protein. One should also consider the possibility that dynamic exchanges are more intrinsic to the ECFP chromophore and its nearby protein matrix and lead to unusual kinetic laws of fluorescence emission. Indeed, a complex situation may arise if the dynamic exchanges, instead of being slow, take place significantly on the nanosecond time scale, and moreover if they are accompanied by a time dependence (on the same time scale) of the nonradiative rates. For example, excited-state torsions of the GFP chromophore, associated with a loss of electronic conjugation, have been described as the major nonradiative process in model compounds (*45*) and may lead in certain cases to nonexponential fluorescence decay profiles (*33, 46*). Further theoretical and experimental investigations will be required to evaluate the possibility and consequences of similar mechanisms taking place on the nanosecond time scale within the ECFP protein.

Consequences for Quantitative Fluorescence Imaging. The fluorescence properties of ECFP expressed in the cytosol of living cells are remarkably similar to those determined for the purified, isolated ECFP at neutral pH. On the other hand, as shown by our parallel intracellular measurements, the strong temperature and pH sensitivity of ECFP and its related variants will have important practical consequences for their use in quantitative imaging of living cells. Well above the reported transition point at pH 5, significant decreases in ECFP fluorescence intensity and lifetime are to be expected, for example, upon moderate local acidosis, or at sites of local production of protons such as in oxidative and ion transport activities. On the other hand, the temperature dependence of ECFP fluorescence can lead, for example, to a 40% change in lifetime and intensity when samples are heated from 20 to 37 °C, or to variations greater than 2%, when the sample temperature is not controlled to better than 1 °C around 20 °C. Thus, temperature variations will be a prominent source of inaccuracy and loss of sensitivity in FRET experiments, where fluorescence intensities or lifetimes are to be compared within a few percent.

CONCLUSION

The results presented here have first a direct relevance to the use of ECFP in quantitative imaging, in terms of designing the experiment, ensuring the highest reproducibility of results, and improving the reliability of data interpretation. On the other hand, the accurate evaluation of the spectroscopic consequences of the single H148D mutation in ECFP sheds some light on the relationships between the protein structure and its fluorescence properties. The intricate complexity and sensitivity of ECFP fluorescence to experimental and physicochemical parameters still awaits a proper and necessarily complex photophysical description. Elaborating a comprehensive model is out of reach for the moment, as it requires further biochemical, structural, spectroscopic, and theoretical studies. However, such a comprehensive description would be a major advance in the understanding of the emissive properties of fluorescent proteins and may have broad implications for their quantitative use in intensity-based as well as lifetime-based applications.

ACKNOWLEDGMENT

We thank Nathalie Neyroud and Sophie Dupré for providing CFP-transfected CHO and PLB985 cells, respectively, and Bernard Lévy for stimulating discussions.

SUPPORTING INFORMATION AVAILABLE

Two tables providing the detailed lifetime components of ECFP and ECFP-H148D along emission wavelengths and pH studies at 20 °C, together with their standard deviations. This material is available free of charge via the Internet at http://pubs.acs.org.

REFERENCES

1. Chalfie, M., Tu, Y., Euskirchen, G., Ward, W. W., and Prasher, D. C. (1994) Green fluorescent protein as a marker for gene expression. *Science 263*, 802–805.

2. Tsien, R. Y. (1998) The green fluorescent protein. *Annu. Rev. Biochem. 67*, 509–544.
3. Cubitt, A. B., Heim, R., Adams, S. R., Boyd, A. E., Gross, L. A., and Tsien, R. Y. (1995) Understanding, improving and using green fluorescent proteins. *Trends Biochem. Sci. 20*, 448–455.
4. Wouters, F. S., Verveer, P. J., and Bastiaens, P. I. (2001) Imaging biochemistry inside cells. *Trends Cell Biol. 11*, 203–211.
5. Shaner, N. C., Patterson, G., and Davidson, M. W. (2007) Advances in fluorescent protein technology. *J. Cell Sci. 120*, 4247–4260.
6. Selvin, P. R. (2000) The renaissance of fluorescence resonance energy transfer. *Nat. Struct. Biol. 7*, 730–734.
7. Vogel, S. S., Thaler, C., and Koushik, S. V. (2006) Fanciful FRET. *Sci. STKE 331*, re2.
8. Domingo, B., Sabariegos, R., Picazo, F., and Llopis, J. (2007) Imaging FRET standards by steady-state fluorescence and lifetime methods. *Microsc. Res. Tech. 70*, 1010–1021.
9. Tramier, M., Gautier, I., Piolot, T., Ravalet, S., Kemnitz, K., Coppey, J., Durieux, C., Mignotte, V., and Coppey-Moisan, M. (2002) Picosecond-hetero-FRET microscopy to probe protein-protein Iinteractions in live cells. *Biophys. J. 83*, 3570–3577.
10. Habuchi, S., Cotlet, M., Hofkens, J., Dirix, G., Michiels, J., Vanderleyden, J., Subramaniam, V., and De Schryver, F. C. (2002) Resonance energy transfer in a calcium concentration-dependent cameleon protein. *Biophys. J. 83*, 3499–3506.
11. Rizzo, M. A., Springer, G. H., Granada, B., and Piston, D. W. (2004) An improved cyan fluorescent protein variant useful for FRET. *Nat. Biotechnol. 22*, 445–449.
12. Kremers, G. J., Goedhart, J., van Munster, E. B., and Gadella, T. W. J. (2006) Cyan and yellow super fluorescent proteins with improved brightness, protein folding, and FRET Forster radius. *Biochemistry 45*, 6570–6580.
13. Millington, M., Grindlay, G. J., Altenbach, K., Neely, R. K., Kolch, W., Bencina, M., Read, N. D., Jones, A. C., Dryden, D. T. F., and Magennis, S. W. (2007) High-precision FLIM-FRET in fixed and living cells reveals heterogeneity in a simple CFP-YFP fusion protein. *Biophys. Chem. 127*, 155–164.
14. Bae, J. H., Rubini, M., Jung, G., Wiegand, G., Seifert, M. H. J., Azim, M. K., Kim, J. S., Zumbusch, A., Holak, T. A., Moroder, L., Huber, R., and Budisa, N. (2003) Expansion of the genetic code enables design of a novel "gold" class of green fluorescent proteins. *J. Mol. Biol. 328*, 1071–1081.
15. Seifert, M. H., Ksiazek, D., Azim, M. K., Smialowski, P., Budisa, N., and Holak, T. A. (2002) Slow exchange in the chromophore of a green fluorescent protein variant. *J. Am. Chem. Soc. 124*, 7932–7942.
16. O'Connor, D. V., and Philipps, D. (1984) *Time-correlated single photon counting*, Academic Press, London.
17. Sinnecker, D., Voigt, P., Hellwig, N., and Schaefer, M. (2005) Reversible photobleaching of enhanced green fluorescent proteins. *Biochemistry 44*, 7085–7094.
18. Grailhe, R., Merola, F., Ridard, J., Couvignou, S., Le Poupon, C., Changeux, J. P., and Laguitton-Pasquier, H. (2006) Monitoring protein interactions in the living cell through the fluorescence decays of the cyan fluorescent protein. *ChemPhysChem 7*, 1442–1454.
19. Merola, F., Rigler, R., Holmgren, A., and Brochon, J. C. (1989) Picosecond tryptophan fluorescence of thioredoxin: Evidence for discrete species in slow exchange. *Biochemistry 28*, 3383–3398.
20. Couprie, M. E., Merola, F., Tauc, P., Garzella, D., Delboulbe, A., Hara, T., and Billardon, M. (1994) First use of the UV Super-ACO free electron laser: Fluorescence decays and rotational dynamics of the NADH coenzyme. *Rev. Sci. Instrum. 65*, 1485–1495.
21. Valeur, B. (2006) *Molecular Fluorescence. Principles and applications*, 3rd ed., Wiley-VCH, Weinheim, Germany.
22. Livesey, A. K., and Brochon, J. C. (1987) Analyzing the distribution of decay constants in pulse-fluorometry using the maximum entropy method. *Biophys. J. 52*, 693–706.
23. Becker, W., Bergmann, A., Hink, M. A., Konig, K., Benndorf, K., and Biskup, C. (2004) Fluorescence lifetime imaging by time-correlated single-photon counting. *Microsc. Res. Tech. 63*, 58–66.
24. Spriet, C., Trinel, D., Waharte, F., Deslee, D., Vandenbunder, B., Barbillat, J., and Heliot, L. (2007) Correlated fluorescence lifetime and spectral measurements in living cells. *Microsc. Res. Tech. 70*, 85–94.
25. Borst, J. W., Hink, M. A., van Hoek, A., and Visser, A. J. W. G. (2005) Effects of refractive index and viscosity on fluorescence and anisotropy decays of enhanced cyan and yellow fluorescent proteins. *J. Fluoresc. 15*, 153–160.
26. Blandin, P., Merola, F., Brochon, J. C., Tremeau, O., and Menez, A. (1994) Dynamics of the active loop of snake toxins as probed by time-resolved polarized tryptophan fluorescence. *Biochemistry 33*, 2610–2619.
27. Miyawaki, A., and Tsien, R. Y. (2000) Monitoring protein conformations and interactions by fluorescence resonance energy transfer between mutants of green fluorescent protein. *Methods Enzymol. 327*, 472–500.
28. Ai, H. W., Henderson, J. N., Remington, S. J., and Campbell, R. E. (2006) Directed evolution of a monomeric, bright and photostable version of *Clavularia* cyan fluorescent protein: Structural characterization and applications in fluorescence imaging. *Biochem. J. 400*, 531–540.
29. Malo, G. D., Pouwels, L. J., Wang, M., Weichsel, A., Montfort, W. R., Rizzo, M. A., Piston, D. W., and Wachter, R. M. (2007) X-ray structure of Cerulean GFP: A tryptophan-based chromophore useful for fluorescence lifetime imaging. *Biochemistry 46*, 9865–9873.
30. Zacharias, D. A., Violin, J. D., Newton, A. C., and Tsien, R. Y. (2002) Partitioning of lipid-modified monomeric GFPs into membrane microdomains of live cells. *Science 296*, 913–916.
31. Demchenko, A. P. (2002) The red-edge effects: 30 years of exploration. *Luminescence 17*, 19–42.
32. Laws, W. R., and Brand, L. (1979) Analysis of two-state excited state reactions. The fluorescence decay of 2-naphtol. *J. Phys. Chem. 83*, 795–802.
33. Grabowski, Z. R., Rotkiewicz, K., and Rettig, W. (2003) Structural changes accompanying intramolecular electron transfer: Focus on twisted intramolecular charge-transfer states and structures. *Chem. Rev. 103*, 3899–4031.
34. Jose, M., Nair, D. K., Reissner, C., Hartig, R., and Zuschratter, W. (2007) Photophysics of clomeleon by FLIM: Discriminating excited state reactions along neuronal development. *Biophys. J. 92*, 2237–2254.
35. Jung, G., Wiehler, J., and Zumbusch, A. (2005) The photophysics of green fluorescent protein: Influence of the key amino acids at positions 65, 203, and 222. *Biophys. J. 88*, 1932–1947.
36. Merola, F., Blandin, P., Brochon, J. C., Trémeau, O., and Ménez, A. (1995) Aggregation of *Naja nigricollis* cardiotoxin: Charaterization and quantitative estimate by time-resolved polarized fluorescence. *J. Fluoresc. 5*, 205–215.
37. Garcia, P., Merola, F., Receveur, V., Blandin, P., Minard, P., and Desmadril, M. (1998) Steady-state and time-resolved fluorescence study of residual structures in an unfolded form of yeast phosphoglycerate kinase. *Biochemistry 37*, 7444–7455.
38. Birks, J. B. (1970) *Photophysics of aromatic molecules*, 1st ed., John Wiley & Sons Ltd., London.
39. Demachy, I., Ridard, J., Laguitton-Pasquier, H., Durnerin, E., Vallverdu, G., Archirel, P., and Levy, B. (2005) Cyan fluorescent protein: Molecular dynamics, simulations, and electronic absorption spectrum. *J. Phys. Chem. B 109*, 24121–24133.
40. Visser, N. V., Hink, M. A., Borst, J. W., van der Krogt, G. N., and Visser, A. J. (2002) Circular dichroism spectroscopy of fluorescent proteins. *FEBS Lett. 521*, 31–35.
41. Ai, H. W., Olenych, S. G., Wong, P., Davidson, M. W., and Campbell, R. E. (2008) Hue-shifted monomeric variants of *Clavularia* cyan fluorescent protein: Identification of the molecular determinants of color and applications in fluorescence imaging. *BMC Biol. 6*, 13.
42. Chen, Y., and Barkley, M. D. (1998) Toward understanding tryptophan fluorescence in proteins. *Biochemistry 37*, 9976–9982.
43. Klingen, A. R., Bombarda, E., and Ullmann, G. M. (2006) Theoretical investigation of the behavior of titratable groups in proteins. *Photochem. Photobiol. Sci. 5*, 588–596.
44. Henderson, J. N., Ai, H. W., Campbell, R. E., and Remington, S. J. (2007) Structural basis for reversible photobleaching of a green fluorescent protein homologue. *Proc. Natl. Acad. Sci. U.S.A. 104*, 6672–6677.
45. Maddalo, S. L., and Zimmer, M. (2006) The role of the protein matrix in green fluorescent protein fluorescence. *Photochem. Photobiol. 82*, 367–372.
46. Vallverdu, G., Demachy, I., Ridard, J., and Lévy, B. (2008) Using biased molecular dynamics and Brownian dynamics in the study of fluorescent proteins. *THEOCHEM* (in press).

BI801400D